UAV-based remote sensing of the Super-Sauze landslide: Evaluation and results

U. Niethammer[a]*, M.R. James[b], S. Rothmund[a], J. Travelletti[c], M. Joswig[a]

[a]Institute for Geophysics, University of Stuttgart, Germany
[b]Lancaster Environment Centre, Lancaster University, UK
[c]School and Observatory of Earth Science, University of Strasbourg, France

Abstract

Unmanned aerial vehicles (UAVs) equipped with digital compact cameras can be used to map landslides quickly and at a high ground resolution. Images taken by a radio-controlled mini quad-rotor UAV of the SuperSauze, France landslide have been used to produce a high-resolution ortho-mosaic of the entire landslide and digital terrain models (DTMs) of several regions. The UAV capability for imaging fissures and displacements on the landslide surface has been evaluated, and the subsequent image processing approaches for suitably georectifying the data have been assessed. For Super-Sauze, horizontal displacements of 7 to 55 m between a high-resolution airborne ortho-photo of May 2007 and a UAV-based ortho-mosaic of October 2008 have been measured. Fixed areas of persistent deformation have been identified, producing fissures of different distributions and orientations comparable to glacial crevasses, and relating directly to the bedrock topography. The UAV has demonstrated its capability for producing valuable landslide data but improvements are required to reduce data processing time for the efficient generation of ortho-mosaics based on photogrammetric DTMs, in order to minimise georeferencing errors.

1 Introduction

In order to monitor hazards from active landslides and to understand the processes involved, both spatial and temporal measurements such as displacement rates and extents and changes in the surface topography are required. For these, remote sensing has been an integral method of landslide investigations for many decades, with several different techniques being used. For example, differential InSAR (Interferometric Synthetic Aperture Radar) enables detailed displacement analysis (Belardinelli et al., 2003), although signal decorrelation due to vegetation changes and sedimentological processes can prevent its use on active landslide surfaces. Passive space-borne imaging is becoming increasing useful for landslide studies; panchromatic QuickBird satellite images can provide data at a ground resolution of 0.61 m and a repeat acquisition interval of down to 3-4 days (Niebergall et al., 2007). Airborne and terrestrial geodetic LIDAR-scans (Light Detection and Ranging) are powerful tools for rapidly collecting high densities of precise and high-resolution 3D surface point coordinates. The quality of such point clouds is mainly influenced by the roughness and reflectivity of the surface, the measurement incidence angle and the observation range (Cheok et al., 2002; Lichti et al., 2005). From point clouds, high-resolution digital terrain models (DTMs) can be derived with accuracies in the submetre range and, in many cases, surface topography can be determined even in vegetated environments (Carter et al., 2007; van den Eeckhaut et al., 2007). Airborne images can provide important surface textural data, but photogrammetric DTMs are not usually as accurate and precise as airborne LIDAR-based DTMs (Baltsavias, 1999) and topography covered by dense vegetation cannot be reconstructed. Traditional airborne- and satellite-based remote sensing techniques are suitable

*Corresponding author: uwe.niethammer@geophys.uni-stuttgart.de

for landslide detection over areas of multiple square kilometres (Henry et al., 2002). For the Super-Sauze landslide studied here, the geomorphological evolution between 1950 and 1995 has been previously reconstructed from 6 airborne ortho-photographs (1 m ground resolution) and the 6 corresponding DTMs (15 m grid) (Weber and Herrmann, 2000). However, these data were of neither sufficient resolution nor repeat rate to resolve the evolution of small landslide features, such as fissure structures or small displacements, which can provide significant information on landslide dynamics.

Here, we investigate the use of radio controlled unmanned aerial vehicles (UAVs) for making such high-resolution measurements of landslides. The mini-UAV used has the advantage over traditional methods of allowing flexible deployments capable of acquiring both high-temporal and spatial resolution data. Radio controlled UAVs are less expensive with significantly lower operational costs than manned aircraft and, in recent years, mapping and remote sensing applications of UAV-systems have become more common (Everaerts, 2008). In the late 1970s the use of fixed wing remote controlled aircraft was investigated for motorised UAV photogrammetry experiments (Przybilla and Wester-Ebbinghaus, 1979) and, a quarter century later, Eisenbeiss et al. (2005) generated the first high-resolution digital terrain models (DTMs) using autonomously controlled helicopter UAVs.

Currently, a range of UAV-systems are in use, for example, motorised paragliders (Jütte, 2008), blimps (Gomez-Lahoz and Gonzalez-Aguilera, 2009), kites (Aber et al., 2002) and balloons (Fotinopoulos, 2004). However, many such systems are strongly affected by wind and could only be used infrequently or with difficulty in mountainous terrain. The availability of small high-quality digital cameras has now enabled radio controlled UAV-systems to represent affordable and practical remote sensing platforms, but data analysis challenges remain. For example, in order to utilise standard aerial photogrammetric processing software, UAV-acquired photographs should be acquired in an optimal block configuration alignment, with internally stable camera-systems and minimal optical distortion. These restrictions have previously required the use of fixed-lens SLR cameras, expensive autopilot UAV navigation systems, and driven the development of dedicated photogrammetric software packages (Eisenbeiss et al., 2005).

In 2006, relatively stable quad-rotor helicopter systems became available as open source public domain projects (Mikrokopter, 2010). These systems are suitable for adaptation for use in alpine terrain and are low-cost when compared to commercially available UAV-systems. The goal of this study was to evaluate a UAV-system developed inhouse for landslide research. Here, we report on the potential and limitations of such a system, with preliminary results acquired from the Super-Sauze landslide, France. For Super-Sauze, a specific aim was to consider the UAV capability for imaging fissures and displacements on the landslide surface and to assess the subsequent image processing approaches for suitably georectifying the data. Fissures on the Super-Sauze landslide have not been mapped in detail in the past and, although this could be carried out by traditional surveying techniques, the large area of the landslide makes remote sensing an appealing technique for this task. With most fissures around 0.1 m in width, they are not resolvable in satellite data and only imaged infrequently by manned airborne systems. Thus, a UAV-system could offer the opportunity for regular data at a suitable resolution to detect changes in the fissure systems.

For full coverage of the landslide area, a plane-rectified orthomosaic of UAV imagery has been constructed and comparisons were made with a previously acquired traditional aerial ortho-photo. However, the use of plane-rectification can result in significant errors in regions of rugged topography, so we explore the application of close range photogrammetry software to enhance the results with a photogrammetric DTM. The close range software can handle convergent imagery from non-metric cameras much more readily than tradi-

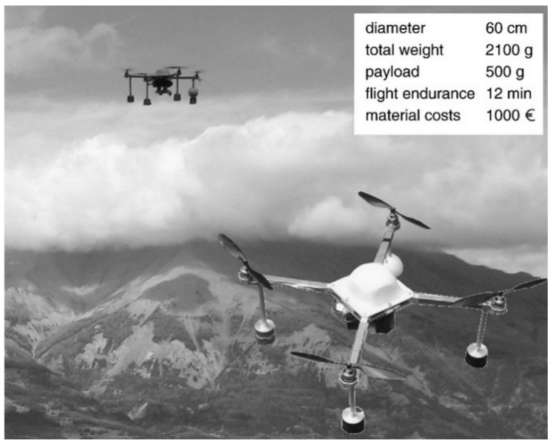

Fig. 1. Quad-rotor system for remote sensing and its main characteristics.

tional aerial photogrammetry applications, facilitating DTM generation from UAV imagery. The quality of the digital terrain model is assessed by comparison with data from a terrestrial laser scanner (TLS).

2 UAV-system

The UAV-system developed in-house is a low-cost quad-rotor (Figure 1) that has been previously demonstrated to be capable of flying in difficult alpine terrain. When compared to conventional helicopters, quad-rotor systems are more stable with less in-flight vibration and have the mechanical advantage of not requiring a large, variable pitch rotor-unit. Our system was derived from an open source project (Mikrokopter, 2010) and enhanced for landslide studies. A robust aluminium flight frame was developed and the payload of the UAV-system was increased by using more powerful motors and some modifications of the flight control software. The UAV is stabilised by inertial measurement units (IMUs), including three acceleration sensors, three gyroscopes, a three-axis compass, and a pressure sensor, regulated by basic PID (proportional integral differential) loops. Flight endurance (hovering time of the UAV-system) is up to 12 min using a lithium polymer battery with a capacity of $\sim$5.0 Ah. Overall UAV-development took about one man year in order to meet all the requirements for operation in difficult alpine terrain. For image acquisition, a light weight low-cost digital compact camera (Praktica Luxmedia 8213) which supports manual camera settings was used. For all flights the sensitivity, zoom and the aperture were set to fixed values in order to achieve exposure times <1/800 s and the largest visual angle. Without an auto-pilot navigation system to control image acquisition, all photographs were taken in an automatic image-series mode, acquiring one image every 3 s to ensure full coverage.

Our choice of a radio controlled UAV requires the presence of a highly skilled pilot and limits the operational area to the control range of a few hundreds of metres. There are also challenges related to the relatively small payloads, UAV-reliability and the restricted radiobandwidth for ground communication (Colomina et al., 2007). Although the use of an autonomously controlled UAV could significantly increase the operational area, autonomous control is less able to cope with unpredictable conditions such as gusty winds than an experienced operator. Furthermore, the use of autonomous UAVs is tightly regulated by civil aviation and security authorities, preventing their practical deployment. Our experience is that, particularly in alpine terrain, UAV-based image acquisition requires significant technical skill and a good UAV pilot.

3 Study area and data acquisition

The study was carried out on the Super-Sauze landslide (Figure 2), located on the north-facing slope of the Barcelonnette Basin (Southern French Alps). The landslide has developed in a torrential basin located in the upper part of Sauze torrent, on the left side downstream of the Ubaye valley and is one of several that have been persistently active since the 1970s. The landslide extends over a horizontal distance of 850 m between elevations of 2105 m at the crown, and 1740 m at the toe, with an average slope of 25°. The landslide mainly consists of

Fig. 2. Location of the study area and upward view of the Super-Sauze landslide. Picture was taken in summer 2006.

Jurassic black marls and has a total volume estimated at 750,000 m^3. Displacement velocities of the unstable slope range from 0.01 m to 0.4 m per day (Malet et al., 2002; Malet et al., 2005).

In October 2008 a UAV flight campaign was carried out covering the whole sliding area (850 $\times$ 250 m) of the Super-Sauze landslide, acquiring 1486 airborne photographs. Flight planning was carried out in-situ, where the area to be imaged could be observed and suitable locations for takeoff and landing could be identified. After launch, the quad-rotor was guided to an imaging flight altitude of $\sim$200 m to provide a ground resolution of approximately 0.06 m per pixel. However, manual control of the UAV led to deviations in flight altitude between 100 m and 250 m, with corresponding ground resolutions between 0.03 m and 0.08 m. At the imaging altitude the UAV was hovered for about 30 s before vertical landing was initiated. After each flight, the area covered by the acquired photographs was verified on the camera directly. To enable the images to be georeferenced, 199 targets ($\sim$0.4 $\times$ 0.6 m rectangular coloured sheets to ensure visibility) were deployed over the landslide as ground control points (GCPs), and their centroid locations determined with differential GPS (DGPS). Deploying such a number of GCPs requires significant effort but was deemed an appropriate precaution for the initial assessment of UAV use over the landslide. Although long-term DGPS observations of these targets could allow for accurate displacements analysis at each GCP without the need for any UAV flight, such point data could potentially miss areas of interest and would not provide opportunity for the analysis of surface features such as fissures.

To enable a comparison of the UAV results with ground-based data, the topography of the toe-region of the slide was also mapped with a terrestrial laser scanner (TLS). The TLS instrument, an Optech ILRIS-3D, was used from a single site at a mean distance of 150 m from the toe (Figure 3A), producing an average data density of 23,000 points per m^2 in the image plane perpendicular to the line of sight, and a total of 3×10^6 points. The laser logged the last return from each line of sight in order to minimise undesired returns from vegetation. A stable area outside of the landslide was also included within the scanned area in order to georeference the TLS data. This georeferencing was carried out using a DTM acquired by airborne LIDAR on 22 May, 2007 and supplied by the company SINTEGRA. A traditional aerial ortho-photo from the same overflight, with a ground resolution of 0.2 m, was also provided by SINTEGRA and this has been used to determine displacements in conjunction with our UAV imagery.

4 Data processing

To allow comparison of the UAV data with these other sources, two processing procedures were carried out; generation of an orthomosaic and DTM construction of selected areas using close range photogrammetry techniques.

4.1 Ortho-mosaic

Previous work has shown that a straightforward plane image rectification approach can be used to produce ortho-mosaics suitable for displacement analysis, analysis of soil moisture, as well as an analysis of fissure structures (Niethammer et al., 2009). Here, the best 59 suitable UAV-acquired images were selected for mosaic processing. In a first step, optical (barrel) distortion was corrected using the

common third degree polynomial approach (Niethammer et al., 2009). In a second processing step, each image was rectified onto the plane GCP coordinates using one of four non-parametric rectification approaches (projective transformation, piecewise affine transformation and polynomial transformations of the 2nd and 3rd order). For each image, the rectification approach was selected in order to achieve the best result and depended on the relief variation and the number of observed ground control points. In irregular terrain these approximate transformations will not fully account for the effects of relief and residual misalignments within the ortho-mosaic have to be accepted. Finally, all rectified photographs were merged to a uniform high-resolution ortho-mosaic with a spatial resolution of 0.04 m. Automatic colour correction was carried out within OrthoVista software (OrthoVista, 2010) by applying a global tiling adjustment function which compares overlapping areas of images and then computes radiometric adjustment parameters for each image. All images were then merged into a seamless mosaic by an adaptive feathering image blending algorithm within OrthoVista (Figure 3A).

4.2 Photogrammetric DTM

DTM generation was carried out using VMS close range photogrammetry software (VMS, 2010) and an image matching algorithm, GOTCHA (Gruen Otto-Chau) from the University College London (Otto and Chau, 1989). Three regions of the Super-Sauze landslide were analysed (Figure 3), representing the areas best covered by multiple images. Two of these cover the upper reaches (DTM 1 and 2, Figure 3B and C, from 10 and 6 images respectively) and one covers the toe-region (DTM 3, Figure 3D, from 30 images). With TLS data only covering the toe-region, the DTM analysis was restricted to DTM 3 of the toe-area.

For DTM creation, observations of ground control points in the selected images were used to calculate initial camera orientations (positions and pointing directions) using a preliminary estimated camera model defining principal distance only. The photogrammetric network produced was densified by incorporating additional tie points generated with GOTCHA. GOTCHA is a dense matching algorithm capable of generating patch-based (rather than featurebased) matches for each pixel of an image. The output was then reduced to a few thousand matches distributed over the images and a self-calibrating network adjustment was carried out in which the errors in the GCP positions, camera orientations and the camera model (principal distance, two radial and two tangential distortion components, principal point offsets and an affinity term) were simultaneously minimised. The optimised locations for the 16 GCPs in the toe-region (Figure 3A) showed RMS position residuals (from the original GCP coordinates) of 0.023, 0.018 and 0.019 m in x, y, and z. As is standard in rigorous close range photogrammetry procedures, VMS calculates the measurement precision within the photogrammetric network (Cooper and Robson, 2001). Average precisions for all the GCPs were 0.079, 0.079 and 0.185 m in x, y, and z, reflecting mean image residuals of 1.4 pixels in both x and y. Such precisions and residual magnitudes are poorer than it is possible to achieve with oblique photogrammetric networks of environmental scenes; for example, over similar observation distances, Chandler et al. (2002) obtained control point measurement precisions that were generally <20 mm for monitoring river channel change. However, such results generally require careful image acquisition planning and the use of an SLR camera, options that are not available when using small, manually controlled UAVs. Nevertheless, compact cameras have been shown to have sufficiently stable imaging geometries for photogrammetric work (Wackrow et al., 2007) and precisions of 20 mm may exceed the requirements of remote sensing of mass-movement phenomena.

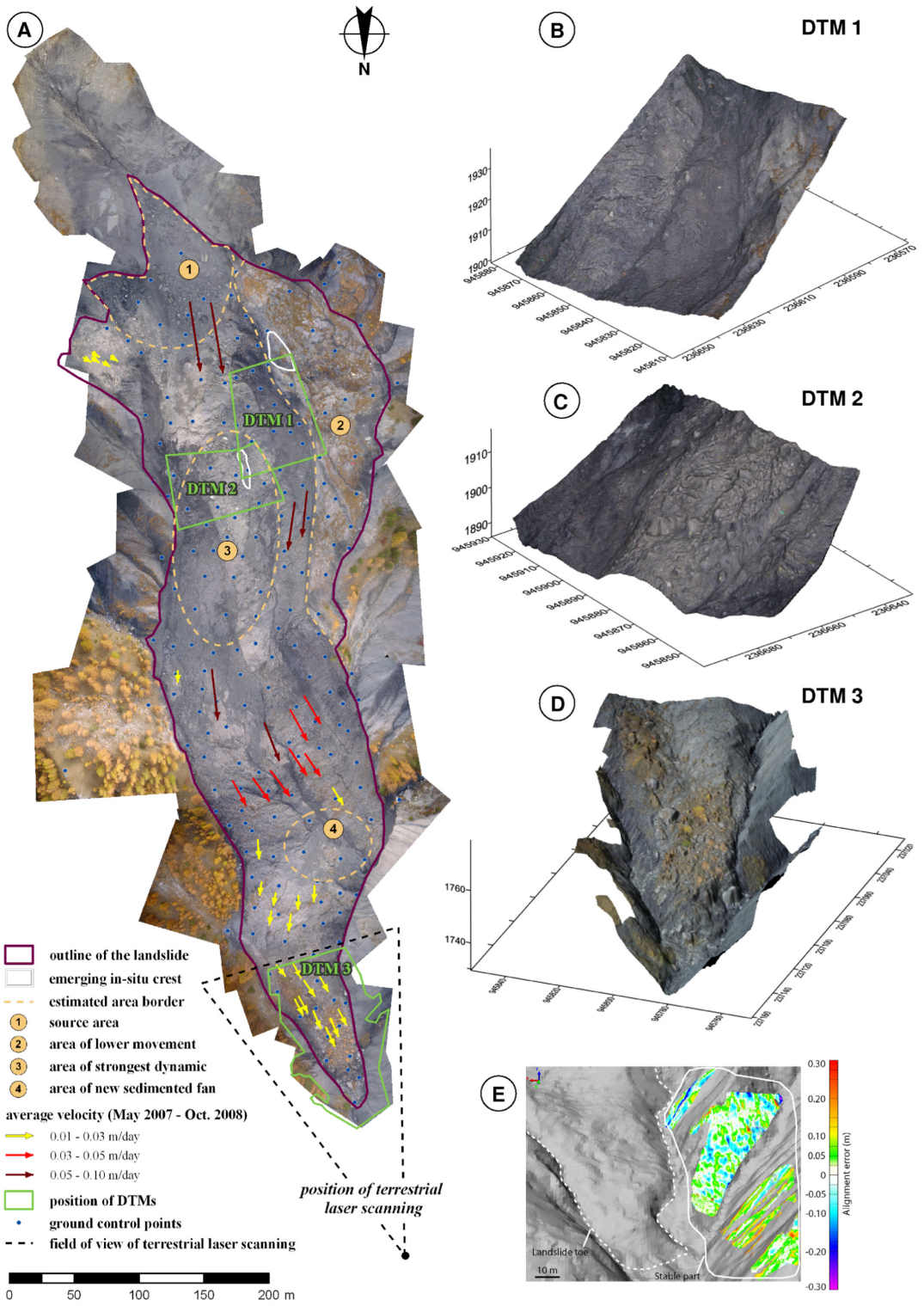

Fig. 3. A: Ortho-mosaic of the Super-Sauze landslide of October 2008 with ground control points (GCPs), horizontal surface displacement vectors colour coded by average movement velocity (May 2007-October 2008), different areas of dynamics and sedimentation, locations of the DTMs and the position and field of view of the terrestrial laser scanner survey. B-D: DTM 1-3 overlain with an ortho-image. E: Alignment error between the TLS DTM (October 2008) and airborne LIDAR DTM (May 2007) of the stable topography adjacent to the toe-region of the landslide.

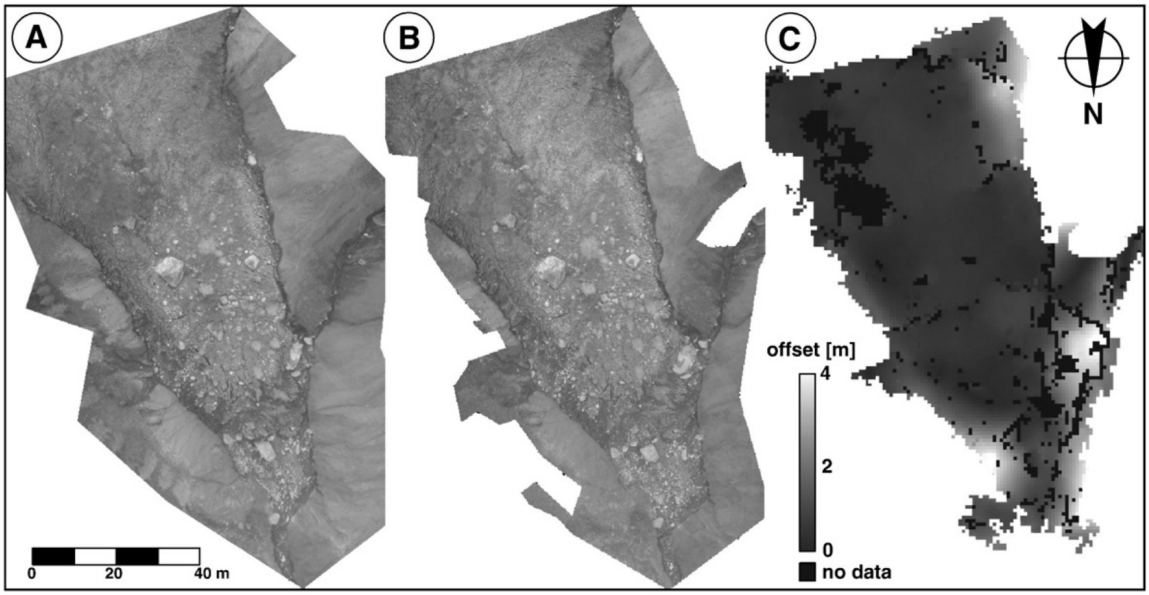

Fig. 4. Comparison between the ortho-mosaic (A) and a DTM-derived ortho-photo (B) of the toe-region. (C) Horizontal offsets determined by GOTCHA image matching.

For example, the precisions here are better than those required and achieved by James et al. (2007) who used a ground-based SLR for assessing lava flows. In future work, one of the easiest ways to increase the precision of the UAV-based DTMs would be to reduce the size of the GCP targets, which were not originally selected for use with VMS. The algorithms in VMS to automatically locate control target centroids are optimised for use with circular retroreflective targets (Robson and Shortis, 1998) and perform best when targets are 5 to 10 pixels across in images. Consequently, centres of the large, rectangular GCPs are not as accurately located within the images as they could be, and GCP residual errors would probably be reduced if smaller, circular targets were employed.

For the creation of DTM 3, 17 of the 30 images in the network overlapped suitably to contribute to the final surface model. After image matching, the output was refined by eliminating outliers, weak matches (e.g. points with significant residuals, poor precisions or matched in only two images) and points clearly influenced by vegetation cover. The resulting point clouds were then interpolated over a 0.2 m grid using kriging in Surfer software (Surfer, 2010).

4.3 Terrestrial laser DTM

TLS data processing was performed using Polyworks software (Polyworks, 2010). The landslide surface is nearly free of vegetation. Trees, stumps and bushes were easily identifiable in the TLS point clouds and could be removed manually without any automatic filtering. In some minor parts of the landslide toe, sparse vegetation, such as grass (less than 0.1 m high) was present. Its effect on the elevation accuracy is smoothed by a 0.2 m grid interpolation, thus leading to a maximum error less than 0.1 m in elevation. However, many automatic filtering methods can be used to remove vegetation (Prokop and Panholzer, 2009). They are useful when vegetation is dense and the affected point cloud covers a large area which was not the case in the present study. Georeferencing was achieved by aligning stable topography adjacent to the landslide to equivalent data in the 2007 airborne LIDAR DTM (Figure 3E). This was carried out using an automated iterative closest point algorithm (ICP), with an initial manual alignment to ensure that the ICP did

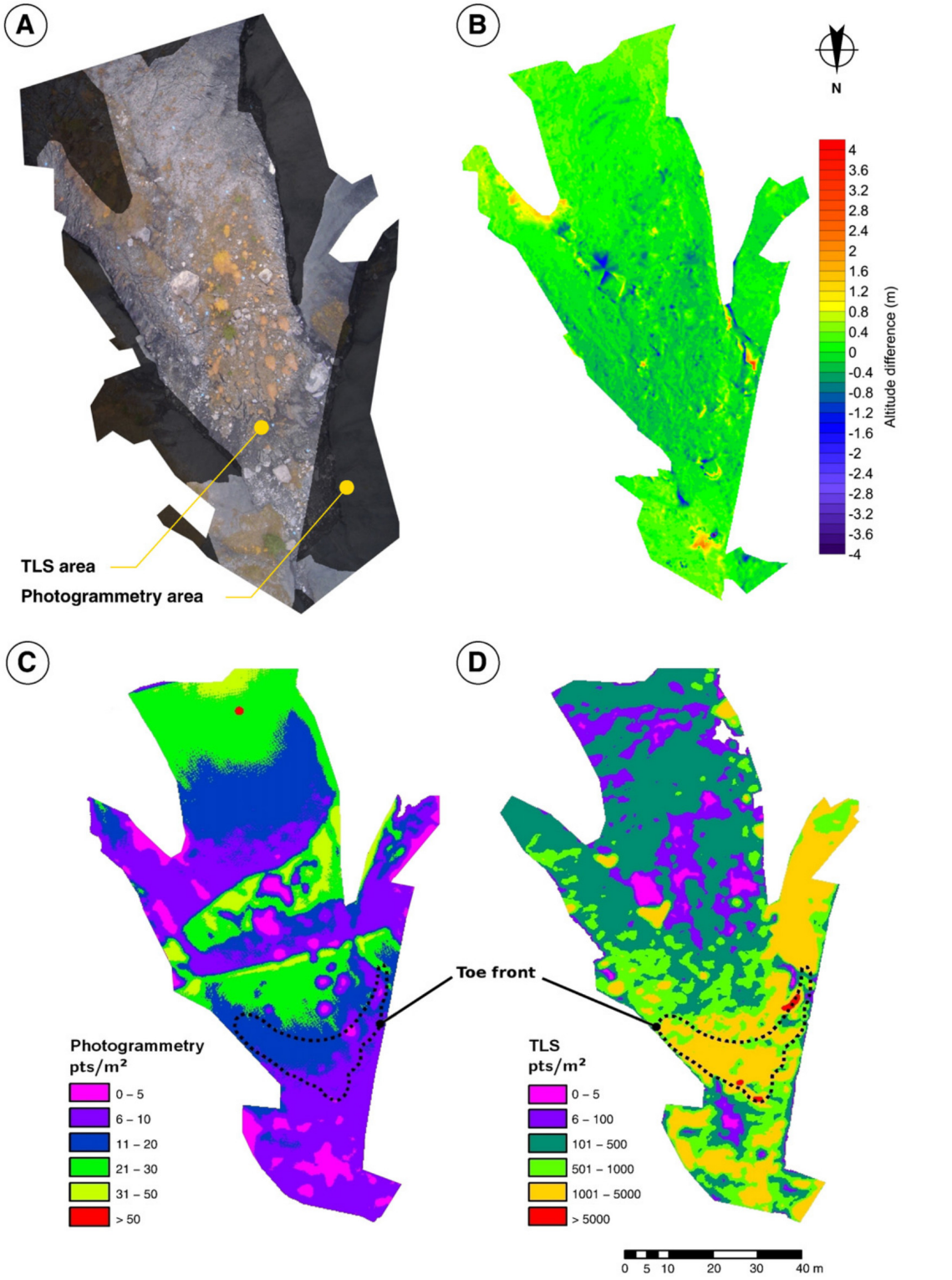

Fig. 5. DTM precision analysis at the toe-region; A: texture of the toe-region, B: elevation differences between TLS and photogrammetric DTM, C: point-density of the photogrammetry data, and D: point-density of the TLS data.

not converge on a local minimum (Lee et al., 1999). This georeferencing method is often applied in areas where access is difficult and where precise GCP reflectors cannot be readily installed, issues typical of landslide areas where slopes of more than 60° can be present (Travelletti et al., 2008; Oppikofer et al., 2009). After alignment, the mean 3D misfit in the stable area was quantified to be 0.05 m with a standard deviation of 0.16 m. The TLS data were then resampled and interpolated to generate a DTM with a 0.2 m grid.

5 Results and discussion

5.1 Ortho-mosaic and DTM quality

Errors within the georeferencing of the ortho-mosaic were quantified by comparison of all 199 GCP locations to their DGPS-measured locations. Within the boundary of the sliding area the mean error was 0.5 m, with a standard deviation of 0.57 m and a maximum misalignment of 3.9 m. However, large misalignments between 2.0 m and 3.9 m were only located at the margins of the landslide and, away from the boundary, accuracies can be considered to be ∼0.5 m. In the toe-region, the ortho-mosaic could also be compared with UAV images ortho-rectified within VMS software using the photogrammetry-derived DTM 3 (Figure 3D). Horizontal offsets were determined by image matching (using GOTCHA) and show similar magnitudes to those of the full ortho-mosaic GCPs (Figure 4A), with the largest values located near the slide boundary.

The quality of the photogrammetric DTM was assessed by subtracting the overlapping TLS DTM (Figure 5A and B). In the vertical direction the RMS difference is 0.31 m although maximum deviations reach +3.44 to -4.08 m. The most significant errors are induced by some small trees and bushes, the effects of which could not be reliably removed from the photogrammetric DTM. However, vegetation correction on landslides has been managed by applying non-uniform vegetation-height surfaces (Martha et al., 2010), but such procedures were not warranted in this work because the most significant vegetation errors were localised and occurred only at the margins of the DTMs. Further sizable differences occur on the steepest sides of large blocks. On the northern faces, where the block surface is nearly perpendicular to the TLS line of sight (Figure 3A), the TLS point cloud is much denser than the photogrammetric one. For example, Figure 5C and D shows that in the steep front of the toe, the point cloud of the TLS is two orders of magnitude denser than the point cloud of the photogrammetry.

However, the TLS can only observe one side of a block and the other, shadowed, side has to be interpolated. In shadow areas, the zero point density results in predicted elevations that reflect the interpolation technique used rather than any real measurements (Figure 6C). Nevertheless, such regions are observed fully by the UAV.

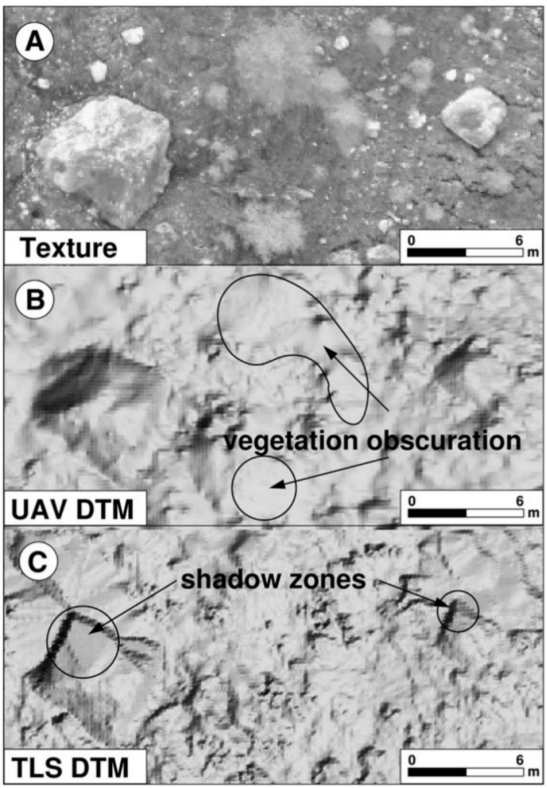

Fig. 6. DTM artefacts resulting from shadow zones in TLS data and vegetation obscuration in the UAV-based DTM.

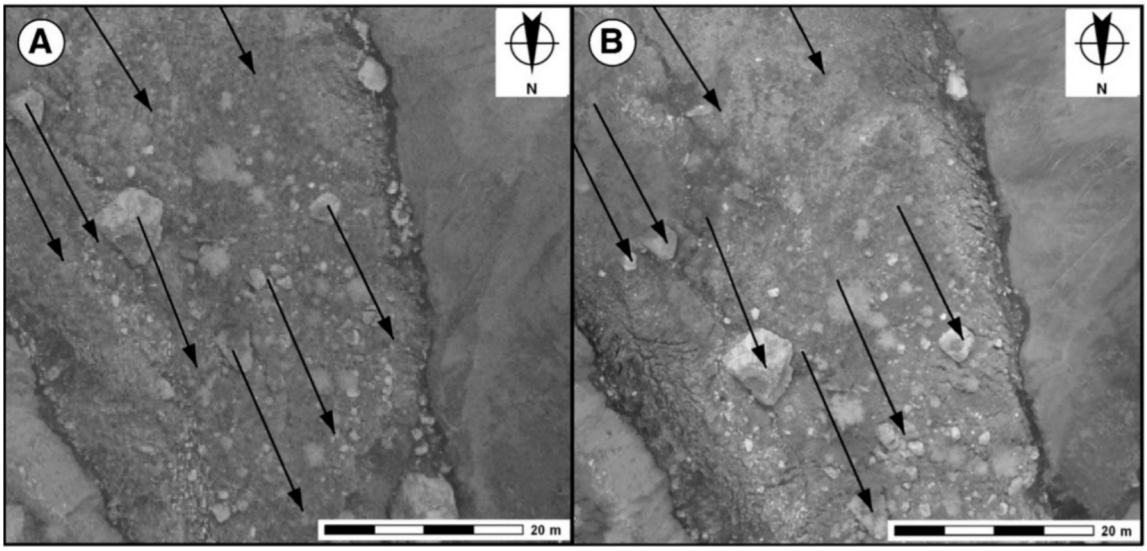

Fig. 7. Horizontal displacement analysis of the toe-region between the airborne ortho-photo of May 2007 (A) and the UAV-based ortho-mosaic of October 2008 (B).

In regions of low vegetation, such as grass or small shrubs, it is difficult to completely remove vegetation returns from the TLS point cloud and this can lead to some small artefacts in the TLS DTM (Figure 6A and C). On the other hand the photogrammetric approach can fail in areas of low image contrast or shadowing (for example, on some large blocks, Figure 6A and B). Dense vegetation cannot be penetrated and can give poor or no results during image matching (Figure 6A and B). It can be concluded that both DTMs must be regarded with caution. Each set of data and method can have advantages and limitations (Kerle, 2002).

5.2 Surface displacements

Our UAV-based displacement analysis of the Super-Sauze landslide was carried out by comparing the ortho-mosaic from October 2008 with the aerial ortho-photo from May 2007 in a geographical information system (GIS). Horizontal displacements were measured by identifying corresponding features and areas, such as rocks, stones and parts of vegetation patches in both images (Figure 7A and B). In principle, such analysis could be attempted by automated image matching (e.g. using correlation-based methods), but due to the resurfacing changes over the 17-month interval, this would be ineffective with the available image pair. However, automated image matching should be possible between UAV-derived orthomosaics acquired at shorter interval periods, and the use of more sophisticated object- or feature-based matching like scale-invariant feature transform (SIFT) could also be investigated (Lowe, 2004; Leprince et al., 2008).

Horizontal displacements between 7 and 55 m $\pm$ 0.5 m, as well as varying displacement directions were detected (Figure 3A). However, several regions could not be successfully analysed due to a lack of clear surface features in both image sets (area 3 in Figure 3A). Comparisons were also prevented in areas of resurfacing by either new fine-grained sediments (the left part of area 3 and area 4, Figure 3A) or the rapid accumulation of both boulders and sediments (particularly in the source region, area 1, Figure 3A). Area 2 (Figure 3A) is characterised by very low velocities, and displacements could not be resolved in this area. Converting all identified displacements to daily average displacement rates gives the range of 0.01 to 0.1 m $\pm$ 1 mm per day for the period between May 2007 and October 2008. In the source area, displacement rates are up

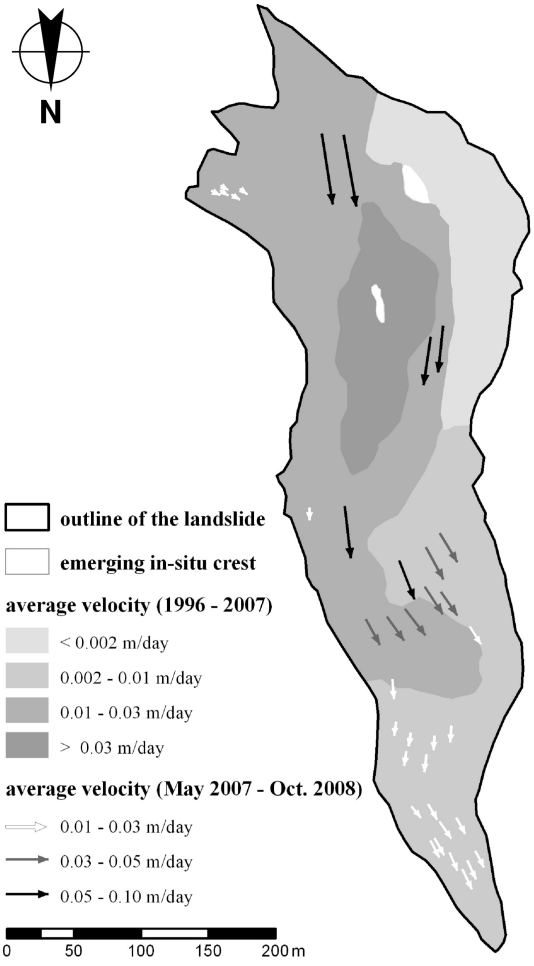

Fig. 8. Horizontal surface displacement vectors (May 2007-October 2008), colour coded by average movement velocity and long-term average movement velocity map (1996-2007), (Amitrano et al., 2007).

to three times greater than to the long-term average (Amitrano et al., 2007) (Figure 8) and approximately two times greater than the average in other regions of the landslide. This suggests that the May 2007 to October 2008 period represented (or encompassed) a period of significantly greater dynamics than normal for the Super-Sauze landslide.

Displacements of the Super-Sauze landslide have been measured on the ground since 1991 by GPS, geodetic and strain instruments (Amitrano et al., 2007). Between 1996 and 2004, average velocities were in the range of 0.002 to 0.03 m per day, but velocities up to 0.4 m per day may be observed each year in the spring season (Amitrano et al., 2007). Monitoring of continuous displacements and pore water pressure have demonstrated that seasonal landslide accelerations are controlled by hydro-climatic conditions and that the long-term behaviour is characterised by continuous movements with a seasonal trend of two acceleration periods (spring and autumn) and two deceleration periods in summer and in winter (Malet and Maquaire, 2003). Such seasonal movement differences cannot be resolved over a 17 month-period. With the capability for providing regular surveys, UAVs could significantly assist in the spatial assessment of landslide displacement. However, despite the high-resolution of the imagery, the general georeferencing accuracy here of ∼0.5 m (resulting from the use of plane-rectification approximations in constructing the ortho-mosaic), could restrict the usefulness of UAV mosaics collected over intervals much shorter than a year. Consequently, effort is required to streamline photogrammetric DTM creation from the UAV images, so that the full landslide area can be efficiently reconstructed and used to increase the accuracy of the orthorectification process.

5.3 Fissures

Many tension- and desiccation cracks and fissures are present on the surface of the Super-Sauze landslide. Tension fissures can be ∼20 m long, up to 0.4 m wide and reach 1 m in depth (Grandjean et al., 2007). In October 2008 most of the fissures were ∼0.1 m in width and are observable in the UAV ortho-mosaic (Figure 9).

Inspection of the fissures in the ortho-mosaic was carried out in a GIS. Despite the downhill movement of the landslide, superficial fissures arise in the same regions of the landslide each year, demonstrating that their locations are controlled by interactions with the paleotopography of the buried bedrock. At the Super-Sauze landslide, longitudinal, transverse, shear, and cross-shaped fissures (Figure 10) have been classified as the principal fissure types (Walter et al., 2009), with their positions

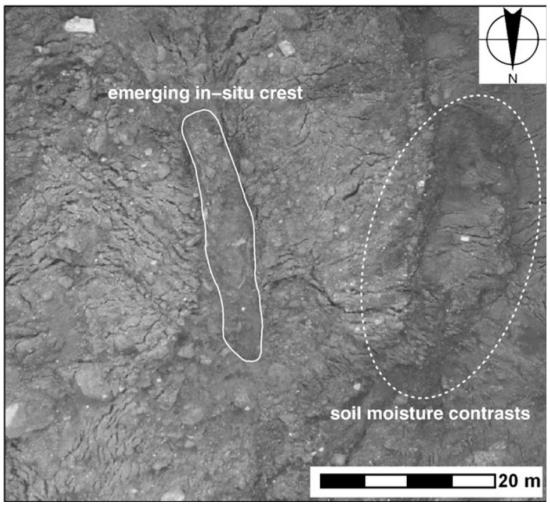

Fig. 9. Emerging in-situ crest, fissures (e.g. shear fissures) and soil moisture contrasts (detail of UAV-based ortho-mosaic of October 2008).

and orientations indicating different styles of deformation and development (Parise, 2003).

Similarities between the observed fissure patterns and those of glacial crevasses suggest a comparable genesis. Landslide dynamics may also be analogous to those of glaciers, resulting from either, or both, sliding and flowing (Kääb, 2002, Malet et al., 2005, Amitrano et al., 2007). Glacial dynamics and crevasses have been well studied (Wilhelm, 1975; Hambrey and Alean, 1994; Hambrey and Lawson, 2000) and crevasse distribution linked to changes in bedrock topography and the lateral bedrock boundaries. For example, longitudinal fissures occur in the direction of movement where an extension of the pathway is initiated. Transverse fissures occur in regions of changes in the decline of the subsurface bedrock slope (Wilhelm, 1975; Varnes, 1978; Hambrey and Alean, 1994). Marginal or shear fissures mostly occur at lateral boundaries between bedrock and the landslide material as result of the velocity gradient (Wilhelm, 1975). In Super-Sauze, such fissures also appear within the landslide material along emerging in-situ bedrock crests (Figures 9 and 10). More intricate fissures, such as crossshaped, may result from a combination of dynamics induced by complex bedrock topography.

Our observations support previous work indicating that stable buried bedrock crests directly affect the behaviour and dynamics of the entire landslide, and that sliding material is 'canalised' by the gullies between crests (Flageollet et al., 2000; Malet, 2003).

Regularly acquired UAV-derived fissure maps could provide valuable spatial data to augment ground-based studies aimed at understanding the links between the sliding material and the bedrock. For example, nanoseismic monitoring can now resolve the low amplitude signals of fracture processes within sedimentary landslide material (Walter et al., 2009 and this issue). Combining these data with high-resolution UAV-based snapshots of fissure distributions and their temporal development could provide valuable insights into the flow dynamics. Furthermore, soil moisture changes suggest to be detectable in contrast variations in UAV images of the landslide surface (Figure 9). This may indicate a promising new approach for high spatial resolution assessment of surface soil moisture, capable of assisting in the quantification of preferred infiltration pathways (for example through fissures), that remains a challenging problem (Krzeminska et al., 2009).

6 Conclusions

In this study it has been shown that radio controlled low-cost UAVs can deliver high-resolution remote sensing data on landslides. The proposed UAV-based remote sensing approach shows significant potential for the production of high-resolution ortho-mosaics and DTMs that enable the analysis of fissures and surface displacements. The manual data acquisition and processing procedures used require a significant amount of time, but progress is already being made to streamline data processing by using automated targetless structurefrom-motion and multiview-stereo approaches to derive the topographic surface (Niethammer et al., 2010). Integrating such DTM generation (which includes camera model re-

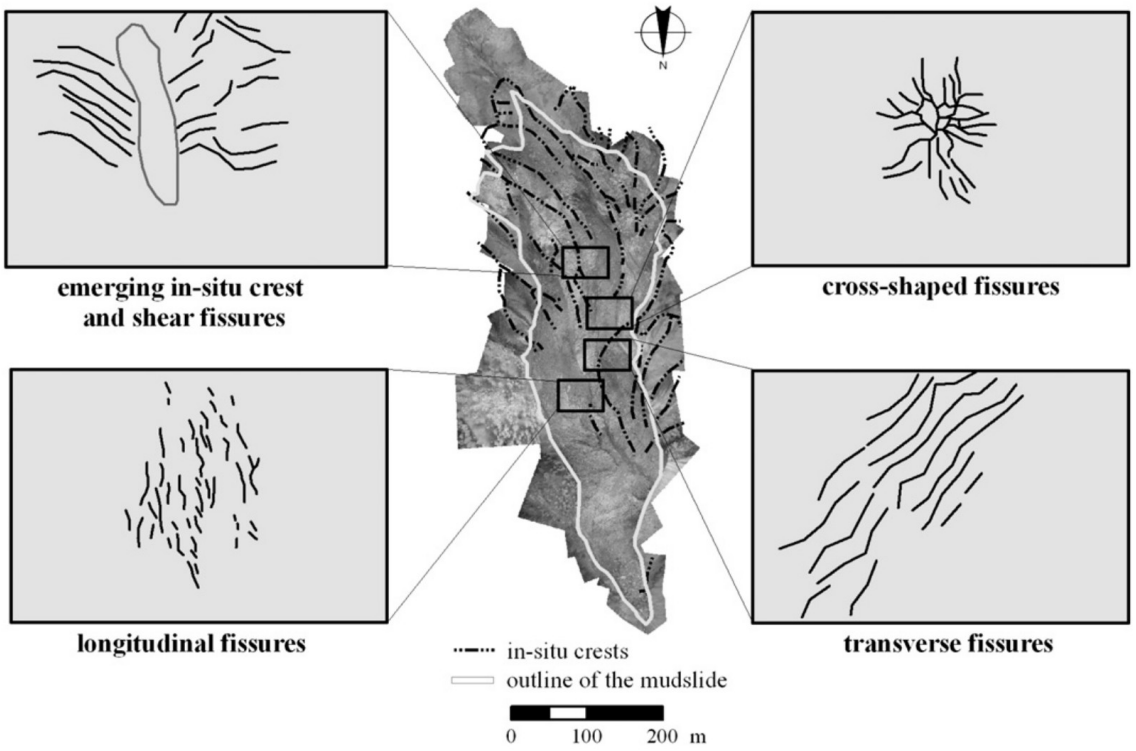

Fig. 10. Principal fissure types: shear fissures, cross-shaped fissures, longitudinal fissures and transverse fissures identified in the ortho-mosaic 2008 of Super-Sauze landslide.

finement), and possibly also vegetation removal, into the ortho-mosaic pipeline, will significantly reduce errors in the final orthomosaic of the Super-Sauze landslide.

The high-resolution of the UAV images and the resulting orthomosaic allowed analysis of fissure patterns and different arrangements (longitudinal, transverse, shear and cross-shaped fissure distributions) were identifiable. The fissures are comparable to glacial crevasses where similar dynamics take place and their patterns reflect the interactions between the sliding material and the bedrock. The UAV imagery thus supports prior observations that buried bedrock crests directly affect the behaviour and dynamics of the entire landslide (Malet, 2003).

The comparison between the plane-rectified UAV ortho-mosaic and an earlier ortho-photo revealed horizontal displacements between 7 and 55 m$\pm$0.5 m, representing daily average displacements rates in the range of 0.1 to 0.01 m$\pm$1 mm per day, between May 2007 and October 2008. Despite the high-resolution of the imagery, errors resulting from the plane-rectification degrade the georeferencing accuracy to $\sim$0.5 m over most of the landslide. Although acceptable when calculating displacement rates over periods of a year, errors of this magnitude would be restrictive for analyses over shorter intervals, and hence could limit the usefulness of the UAV's capability to regularly acquire data.

Consequently, ortho-rectification using photogrammetric DTMs is advised. A DTM of the toe-region of the Super-Sauze landslide, constructed using close range photogrammetry software, has been compared with TLS data of the same area giving an RMS of height difference values of 0.31 m. Although TLS-based point clouds are denser than photogrammetric derived point clouds, TLS data are subject to shadowing due to the oblique view point. Such shadows are minimised in nadir UAV-acquired

images and a large scale data acquisition can be obtained more effectively by UAV.

Acknowledgements

We thank all colleagues from the OMIV project (Observatoire des Instabilités de Versants) for the helpful discussions and their support in the field. The authors are grateful to Jean-Philippe Malet (School and Observatory of Earth Sciences, University of Strasbourg) for providing several datasets. Our thanks also go to Eberhard Claar (Institute for Geophysics, Universität Stuttgart) who built significant components of the quad-rotor systems. The work was supported by the DFG within the project FOR 581 'Natural Slopes' and by the European Commission within the Marie Curie Research Training Network Mountain Risks: from prediction to management and governance (MCRTN-035798). Prof. S. Robson and Prof. J. P. Muller (UCL, London) are thanked for ongoing support through the use of VMS and the Gotcha stereo matching engine respectively. We also like to thank the reviewers for their constructive comments and suggestions.

References

Aber, J.S., Aber, S.W., Pavri, F., 2002. Unmanned small-format aerial photography from kites for acquiring large scale, high-resolution, multiview-angle imagery. Proceedings of Pecora 15, Land Satellite Information IV/ISPRS Conference Commission I/FIEOS, Denver, CO, USA.

Amitrano, D., Gaffet, S., Malet, J.-P., Maquaire, O., 2007. Understanding mudslides through micro-seismic monitoring: the Super-Sauze (South-East French Alps) case study. Bull. Soc. Géol. Fr. 178 (2), 149-157.

Baltsavias, E.P., 1999. A comparison between photogrammetry and laser scanning. ISPRS J. Photogramm. Remote Sensing 54, 83-94.

Belardinelli, M.E., Sandri, L., Baldi, P., 2003. The major event of the 1997 UmbriaMarche (Italy) sequence: what could we learn from DInSAR and GPS data? Geophys. J. Int. 153 (1), 242-252.

Carter, W.E., Shrestha, R.L., Slatton, K.C., 2007. Geodetic laser scanning. Phys. Today 60 (12), 41-47.

Chandler, J., Ashmore, P., Paola, C., Gooch, M., Varkaris, F., 2002. Monitoring riverchannel change using terrestrial oblique digital imagery and automated digital photogrammetry. Ann. Assoc. Am. Geogr. 92, 631-644.

Cheok, G.S., Leigh, S., Rukhin, A., 2002. Technical report: calibration Experiments of a Laser Scanner. US National Institute of Standards and Technology, Report No NISTIR, p. 6922.

Colomina, I., Aigner, E., Agea, A., Pereira, M., Vitoria, T., Jarauta, R., Pascual, J., Ventura, J., Sastre, J., Brechbühler, G.P., Derani, A., Hasegawa, J., 2007. The uVISION project for helicopter UAV photogrammetry and remote-sensing. Proceedings of the 7th Geomatic Week, Barcelona, Spain.

Cooper, M.A.R., Robson, S., 2001. Theory of close range photogrammetry. In: Atkinson, K.B. (Ed.), Close Range Photogrammetry and Machine Vision. Whittles Publishing, Caithness, p. 371.

Van den Eeckhaut, M.V., Poesen, J., Verstraeten, G., Vanacker, V., Nyssen, J., Moeyersons, J., Beek, L.P., Vandekerckhove, L., 2007. Use of LIDAR-derived images for mapping old landslides under forest. Earth Surf. Process. Landforms 32 (5), 754-769.

Eisenbeiss, H., Lambers, K., Sauerbier, M., 2005. Photogrammetric recording of the archaeological site of Pinchango Alto (Palpa, Peru) using a mini helicopter (UAV). Proceedings of the 33rd CAA Conference, Tomar, Portugal, 21-24 March 2005.

Everaerts, J., 2008. The use of unmanned aerial vehicles (UAVs) for remote sensing and mapping. The International Archives of the Photogrammetry. Remote Sensing Spatial Information Sciences XXXVII Part B1, Beijing 2008.

Flageollet,J.-C.,Malet,J.-P.,Maquaire,O.,2000.The 3D structureofthe Super Sauze earthflow: a first stage towards modelling its behaviour. Phys. Chem. Earth 25 (9), 785-791.

Fotinopoulos, V., 2004. Balloon photogrammetry for archaeological surveys. International Archives of the Photogrammetry. Remote Sensing and Spatial Information Sciences, XX ISPRS Congress, Istanbul, Turkey, XXXV-B5, pp. 504-507.

Gomez-Lahoz, J., Gonzalez-Aguilera, D., 2009. Recovering traditions in the digital era: the use of blimps for modelling the archaeological cultural heritage. J. Archaeol. Sci. 36 (1), 100-109.

Grandjean, G., Malet, J.-P., Bitri, A., Méric, O., 2007. Geophysical data fusion by fuzzy logic for imaging the mechanical behaviour of mudslides. Bull. Soc. Géol. Fr. 178 (2), 127-136.

Hambrey, M., Alean, J., 1994. Glaciers. Cambridge University Press, New York.

Hambrey, M.J., Lawson, W.J., 2000. Structural styles and deformation fields in glaciers: a review. In: Maltman, A.J., Hubbard, B., Hambrey, M.J. (Eds.), Deformation of Glacial Materials: Geol. Soc. Spec. Publ., 176, pp. 59-83.

Henry, J.-B., Malet, J.-P., Maquaire, O., Grussenmeyer, P., 2002. The use of small-format and low-altitude aerial photos for the realization of high-resolution DEMs in mountainous areas: application to the Super-Sauze earth-flow (Alpes-de-HauteProvence, France). Earth Surf. Process. Landforms 27 (12), 1339-1350.

James, M.R., Pinkerton, H., Robson, S., 2007. Image-based measurement of flux variation in distal regions of active lava flows. Geochem. Geophys. Geosyst. 8, Q03006. doi:10.1029/2006GC001448.

Jütte, K., 2008. Vergleich verschiedener low-cost Luftbildaufnahmesysteme sowie Einsatz von Drohnen: Grenzen und Möglichkeiten. Bayerische Landesanstalt für Wald und Forstwirtschaft, Der gepixelte Wald - Fachtagung zur Forstlichen Fernerkundung.

Kääb, A., 2002. Monitoring high-mountain terrain deformation from repeated air- and spaceborne optical data: examples using digital aerial imagery and ASTER data. ISPRS J. Photogrammetry Remote Sensing 57, 39-52.

Kerle, N., 2002. Volume estimation of the 1998 flank collapse at Casita volcano, Nicaragua: a comparison of photogrammetric and conventional techniques. Earth Surf. Process. Landforms 27, 759-772.

Krzeminska, D.M., Bogaard, T.A., Debieche, T.-H., Marc, V., Ponton, J., Malet, J.-P., 2009. Quantitative analysis of preferential flow during small scale infiltration tests on an active mudslide, French Alps. In: Malet, J.-P., Remaitre, A., Boogard, T. (Eds.), Proceedings of the International Conference on Landslide Processes: From Geomorphologic Mapping to Dynamic Modelling. CERG Editions, Strasbourg, pp. 151-156.

Lee, B.U., Kim, C.M., Park, R.H., Nurre, J.H., Corner, B.R., 1999. Error sensitivity of rotation angles in the ICP algorithm. SPIE Proc. A 3640, 146-156.

Leprince, S., Berthier, E., Ayoub, F., Delacourt, C., Avouac, J.-P., 2008. Monitoring earth surface dynamics with optical imagery. EOS Transactions American Geophysical Union 89 (1).

Lichti, D.D., Gordon, S.J., Tipdecho, T., 2005. Error models and propagation in directly georeferenced terrestrial laser scanner networks. J. Surv. Eng. 131 (4), 135-142.

Lowe, D., 2004. Distinctive image features from scale-invariant keypoints. International J. Computer Vision 60 (2), 91-110.

Malet, J.-P., Maquaire, O., Calais, E., 2002. The use of Global Positioning System techniques for the continuous monitoring of landslides: application to the Super-Sauze earthflow (Alpes-de-Haute-Provence, France). Geomorphology 43 (1-2), 33-54.

Malet, J.-P., 2003. Les glissements de type écoulement dans les marnes noires des Alpes du Sud. Morphologie, fonctionnement et modelisation hydro-mecanique. Phd thesis, Universite Louis Pasteur, Strasbourg, 364 pp.

Malet, J.-P., Maquaire, O., 2003. Black marl earthflows mobility and long term seasonal dynamic in southeastern France. In: Picarelli, L. (Ed.), Proceedings of the International Conference on Fast Slope Movements: Prediction and Prevention for Risk Mitigation. Bologna, Patron Editore, pp. 333-340.

Malet, J.-P., van Asch, Th.W.J., van Beek, R., Maquaire, O., 2005. Forecasting the behaviour of complex landslides with a spatially distributed hydrological model. Nat. Hazards Earth Syst. Sci. 5 (1), 71-85.

Martha, T.R., Kerle, N., Jetten, V.G., van Westen, C.J., Kumar, V., 2010. Landslide volumetric analysis using Cartosat-1-derived DEMs. IEEE Geosci. Remote Sensing Lett. 7 (3), 582-586.

Mikrokopter, 2010. Mikrokopter Open Source Quad-Rotor Homepage. http://www.mikrokopter.com. (accessed 01.08.2010).

Niebergall, S., Loew, A., Mauser, W., 2007. Object-orientated analysis of very highresolution QuickBird data for mega city research in Delphi/India. Proceedings of the Urban Remote Sensing Joint Event, Paris. ISBN: 1-4244-0712-5. 8 pp., IEEE 07EX1577.

Niethammer, U., Rothmund, S., Joswig, M., 2009. UAV-based remote sensing of the slowmoving landslide Super-Sauze. In: Malet, J.-P., Remaitre, A., Boogard, T. (Eds.), Proceedings of the International Conference on Landslide Processes: From Geomorphologic Mapping to Dynamic Modelling. CERG Editions, Strasbourg, pp. 69-74.

Niethammer, U., Rothmund, S., James, M.R., Travelletti, J., Joswig, M., 2010. UAV-based remote sensing of landslides. Int. Arch. Photogram. Rem. Sens. Spatial Inf. Sciences, vol. XXXVIII. ISPRS Comm. V., Newcastle-upon-Tyne, U.K.

Oppikofer, T., Jaboyedoff, M., Blikra, L., Derron, M.-H., Metzger, R., 2009. Characterization and monitoring of the Aknes rockslide using terrestrial laser scanning. Nat. Hazards Earth Syst. Sci. 9 (3), 1003-1019.

OrthoVista, 2010. Official OrthoVista Software Homepage. http://www.orthovista.com. (accessed 01.08.2010).

Otto, G.P., Chau, T.K.W., 1989. Region-growing algorithm for matching of terrain images. Image Vision Comput. 7 (2), 83-94.

Parise, M., 2003. Observation of surface features on an active landslide, and implications for understanding its history of movement. Nat. Hazards Earth Syst. Sci. 3, 569-580.

Polyworks, 2010. Official Invometric Software Homepage. http://www.inovmetric.com. (accessed 01.08.2010).

Prokop, A., Panholzer, H., 2009. Assessing the capability of terrestrial laser scanning for monitoring slow moving landslides. Nat. Hazards Earth Syst. Sci. 9, 1921-1928.

Przybilla, H.-J., Wester-Ebbinghaus, W., 1979. Bildflug mit ferngelenktem Kleinflugzeug. Bildmessung und Luftbildwesen Zeitschrift fuer Photogrammetrie Fernerkundung 47 (5), 137-142.

Robson, S., Shortis, M.R., 1998. Practical influences of geometric and radiometric image quality provided by different digital camera systems. Photogrammetric Record 16(92),225-248.

Surfer, 2010. Golden Software Homepage. http://goldensoftware.com. (accessed 01.08.2010).

Travelletti, J., Oppikofer, T., Delacourt, C., Malet, J.-P., Jaboyedoff, M., 2008. Monitoring landslide displacements during a controlled rain experiment using a long-range terrestrial laser scanning (TLS). Int. Arch. Photogramm. Remote Sens. 37 (Part B5), 485-490.

Varnes, D.J., 1978. Slope movement types and processes. In: Schuster, R.L., Krizek, R.J. (Eds.), Landslides – Analysis and Control: Rep. Natl. Res. Counc. Transp. Res. Board, vol. 176, pp. 11-33.

VMS, 2010. Official VMS Software Homepage. http://www.geomsoft.com. (accessed 01.08.2010).

Wackrow, R., Chandler, J.H., Bryan, P., 2007. Geometric consistency and stability of consumer-grade digital cameras for accurate spatial measurement. Photogrammetric Record 22 (118), 121-134.

Walter, M., Niethammer, U., Rothmund, S., Joswig, M., 2009. Joint analysis of the SuperSauze (French Alps) mudslide by nanoseismic monitoring and UAV-based remote sensing. EAGE First Break 27 (8), 75-82.

Walter, M., Arnhardt, C., Joswig, M., this issue. Seismic monitoring of rockfalls, subsurface fracture processes, and superficial fissure development at the SuperSauze, French Alps, mudslide. Eng. Geol.

Weber, D., Herrmann, A., 2000. Contribution of digital photogrammetry in spatiotemporal knowledge of unstable slopes: the example of the Super-Sauze landslide (Alpes-de-Haute-Provence, France). Bull. Soc. Géol. Fr. 171 (6), 637-648.

Wilhelm, F., 1975. Schnee- und Gletscherkunde. Walter de Gruyter Press, Berlin, New York.